

Geochemistry, Geophysics, Geosystems



RESEARCH ARTICLE

10.1029/2020GC009064

Tellurium in Late Permian-Early Triassic Sediments as a Proxy for Siberian Flood Basalt Volcanism

Key Points:

- Tellurium is enriched in sediments from the Late Permian Extinction (LPE) to Permian-Triassic Boundary interval in Spitsbergen
- Tellurium and mercury are volcanogenic in origin, Te/Th ratios in sediments may represent a new proxy for volcanism
- Te and Hg imply short time interval for Siberian Traps volcanism, with most intense period initiating at the LPE

Supporting Information:

- Supporting Information S1

Correspondence to:

M. Regelous
 Email: marcel.regelous@fau.de




Citation:

Regelous M., Regelous A., & Grasby S. E., et al. (2020). Tellurium in late permian-early triassic sediments as a proxy for siberian flood basalt volcanism. *Geochemistry, Geophysics, Geosystems*, 21, e2020GC009064. <https://doi.org/10.1029/2020GC009064>

Received 30 MAR 2020
 Accepted 21 OCT 2020

[Correction added on 21 JAN 2021, after first online publication: ProjektDEAL funding statement has been added.]

© 2020. The Authors.
 This is an open access article under the terms of the Creative Commons Attribution-NonCommercial License, which permits use, distribution and reproduction in any medium, provided the original work is properly cited and is not used for commercial purposes.

Marcel Regelous¹ , Anette Regelous¹, Stephen E. Grasby^{2,3} , David P. G. Bond⁴, Karsten M. Haase¹ , Stefan Gleißner¹, and Paul B. Wignall⁵

¹GeoZentrum Nordbayern, Universität Erlangen-Nürnberg, Erlangen, Germany, ²Geological Survey of Canada, Calgary, Canada, ³Department of Geoscience, University of Calgary, Calgary, Canada, ⁴Department of Geography, Environment and Earth Sciences, University of Hull, Hull, UK, ⁵School of Earth and Environment, University of Leeds, Leeds, UK

Abstract We measured the concentrations of trace elements in Late Permian to Early Triassic sediments from Spitsbergen. High mercury concentrations in sediments from the level of the Permo-Triassic Mass Extinction (PTME) at this location were previously attributed to the emplacement of the Siberian Traps Large Igneous Province and used to link the timing of volcanism with the record of environmental change and extinction in these sediments. We investigated the use of the moderately to highly volatile, siderophile elements Ni, Zn, Cd, Sb, Te, Re, and Tl as proxies for the intensity of Siberian volcanism. These trace elements, like Hg, have high concentrations in volcanic gas compared to crustal rocks. Tellurium is highly enriched at the PTME, and Te/Th ratios increase by a factor of ~20 across the PTME, similar to the variation in Hg/total organic carbon (TOC) in the same samples. Te/Th and Hg/TOC values imply that Siberian volcanism initiated at the onset of the PTME, coincident with the start of the $\delta^{13}\text{C}_{\text{organic}}$ excursion and abrupt warming. Based on Te and Hg, most Siberian volcanism occurred between the two phases of the PTME boundary (a period of less than 100 ky), but also continued into the Early Triassic. The duration of Siberian volcanism inferred from Te/Th and Hg/TOC is shorter than that indicated by recent high-precision U-Pb ages of Siberian intrusive and extrusive rocks. Te concentrations and Te/Th ratios in sediments represent a useful new proxy for volcanism, which can be used to link the marine sedimentary record with large volcanic events on land.

1. Introduction

The Permo-Triassic Mass Extinction (PTME) was the most catastrophic biocrisis of the entire Phanerozoic. About 90% of all marine species became extinct near the P-Tr boundary, including all tabulate and rugose corals, trilobites and several brachiopod types, and many other groups including conodonts and ammonoids were severely affected (e.g., Bond & Grasby, 2017; Bond & Wignall, 2014; Erwin, 1994). The main phase of extinction occurred over a short time interval in the latest Permian (e.g., Bond & Grasby, 2017), this Late Permian Extinction (LPE) phase is recorded immediately below bed 25 in the Meishan stratotype section, with a second phase recorded in the basal Triassic at the bed 28/29 boundary at this location (Song et al., 2013). The absolute ages of these horizons are constrained by U-Pb zircon ages of 251.941 ± 0.037 and 251.880 ± 0.031 Ma for beds 25 and 28 respectively (Burgess et al., 2014), a period of 61 ± 48 kyr.

These ages overlap with the ages of flood basalt volcanism in Siberia (251 Ma), at which time $>2 \times 10^6$ km³ of lava were erupted within a few 100 kyr (Bowring et al., 1998; Burgess & Bowring, 2015; Burgess et al., 2014, 2017; Reichow et al., 2009; Renne et al., 1995). The environmental effects of this volcanism are widely accepted to have caused the PTME (e.g., Bond & Grasby, 2017; Bond & Wignall, 2014; Burgess et al., 2017; Korte et al., 2010; Saunders & Reichow, 2009; Wignall, 2015). A large negative excursion in $\delta^{13}\text{C}$ values coincident with the onset of the PTME indicates severe perturbation of the global carbon cycle and has been attributed to release of isotopically light C from Siberian flood basalts and/or metamorphic CO₂ and CH₄ released during sill intrusion into sediments underlying the Siberian flood basalts (Burgess et al., 2017; Grasby et al., 2011; Svensen et al., 2009). Widespread development of marine anoxia (Wignall & Hallam, 1992; Wignall & Twitchett, 1996), and ocean acidification (Beauchamp & Grasby, 2012; Clarkson et al., 2015) resulting from global warming (Joachimski et al., 2012; Sun et al., 2012) and increased weathering and continental runoff (Algeo & Twitchett, 2010), may all have been important factors leading to marine extinction.

Despite the high-quality radiometric ages that now exist both for Siberian volcanic rocks and Permian-Triassic sediments, the short timescale over which flood basalt volcanism, environmental change and extinction occurred, and ambiguities in the stratigraphy of Siberian lavas, means that the relative timing of these events is still unclear. Recent high-precision U-Pb ages for Siberian intrusive and extrusive rocks suggest that volcanism began at or before 252.24 ± 0.12 Ma, and a 4 m-thick sequence of lavas was erupted within a few 100 ky (Burgess et al., 2017). The LPE at 251.902 ± 0.024 Ma coincided with the start of massive intrusive magmatism, followed by a second phase of extrusive volcanism continuing into the Triassic (Burgess et al., 2017).

In order to determine the role of Siberian volcanism during Late Permian-Early Triassic environmental change and extinctions, geochemical proxies for volcanism are needed that can link the sedimentary and volcanic records. Such proxies have the potential to record not only the relative timing of volcanism and environmental and biological changes, but also the intensity of volcanism. Recently, Hg contents and Hg/total organic carbon (TOC) ratios in sediments have been used as a volcanic proxy to link the volcanic and sedimentary records (e.g., Grasby et al., 2015b, 2019; Sanei et al., 2012). As Hg has a strong affinity for organic matter, the Hg/TOC ratio is generally used to account for changes related to increased bioproductivity as compared to enhanced volcanism. High Hg/TOC ratios are associated with several mass extinction events that are thought to have been caused by Large Igneous Province (LIP) volcanism (Grasby et al., 2019), including the PTME (Grasby et al., 2013a, 2013b, 2015b; Sanei et al., 2012; Wang et al., 2018, 2019), but also the end Triassic (Percival et al., 2017) and Early Jurassic events (Fantasia et al., 2019; Percival et al., 2015). However, variations in Hg/TOC in different sediment sections from the same time intervals often differ (e.g., Percival et al., 2015; Shen et al., 2019a; Them et al., 2019). Hg isotope compositions and differences in Hg/TOC between shallow- and deepwater P-Tr sections may indicate that the main source of Hg was from increased continental weathering, rather than directly from volcanism (Grasby et al., 2016, 2019; Them et al., 2019; Wang et al., 2018). Hg/TOC ratios may also be sensitive to sediment mineralogy (e.g., the presence of pyrite; Fantasia et al., 2019; Sanei et al., 2012; Shen et al., 2019a) and to postdepositional alteration (Charbonnier et al., 2020).

Measurements of the composition of volcanic gases emitted from currently active volcanoes show that in addition to Hg, several other volatile trace elements can be highly enriched in volcanic gas, in particular, the trace chalcophile elements Re, Se, Te, Cd, As, Bi, Sb, Tl, and Zn (e.g., Symonds et al., 1987; Zelenski et al., 2013, 2014). The potential of these elements as proxies for volcanism has not yet been explored in any detail, although it has been suggested that several of these elements, like Hg, may have been enriched in P-Tr sediments as a result of Siberian flood basalt volcanism. Rampino et al. (2017) and Rothman et al. (2014) reported Ni enrichments in sediments at the time of the LPE and attributed these to Siberian flood basalt volcanism. High Zn concentrations and light Zn isotope compositions in the carbonate fraction of sediments from the Meishan section have been proposed to result from input of volcanic Zn from Siberian volcanism (Liu et al., 2017).

Compared to Ni and Zn, the chalcophile trace elements Se, Te, As, Sb, Re are enriched in volcanic gas relative to average crustal rocks to a greater extent (Symonds et al., 1987; Zelenski et al., 2013). Provided that these elements have sufficiently long atmospheric residence times and can be transported far from the site of volcanism, their concentrations in marine sediments may potentially be useful as proxies for volcanism. However, other processes can also influence the concentrations of these elements in sediments. For example, the flux of Ni, Zn, and Cd to the sediment increase during periods of higher productivity due to complexation with organic material which accelerates scavenging in the water column (e.g., Tribouillard et al., 2006). Thallium, as well as Mo, U, and V are sensitive to variations in the redox conditions within the sediment and overlying water column, and Zn and Ni together with Pb and Co may be enriched in sediments due to absorption onto Mn-oxyhydroxides in the water column (e.g., Calvert & Pedersen, 1996). Much less is known about the behavior of Te, Se, and Sb which are rarely measured due to their low abundances. In order to determine whether enrichments in chalcophile trace elements in sediments are due to volcanic input, it is important to examine their variations with other elements.

We measured a suite of 43 trace elements, including Ni, Zn, Cd, Sb, Te, Re, and Tl as well as Hg in sediments from the Festningen Section in western Spitsbergen. This location preserves a relatively complete and undisturbed sequence of Late Permian to Early Triassic dominantly clastic sediments which were deposited at

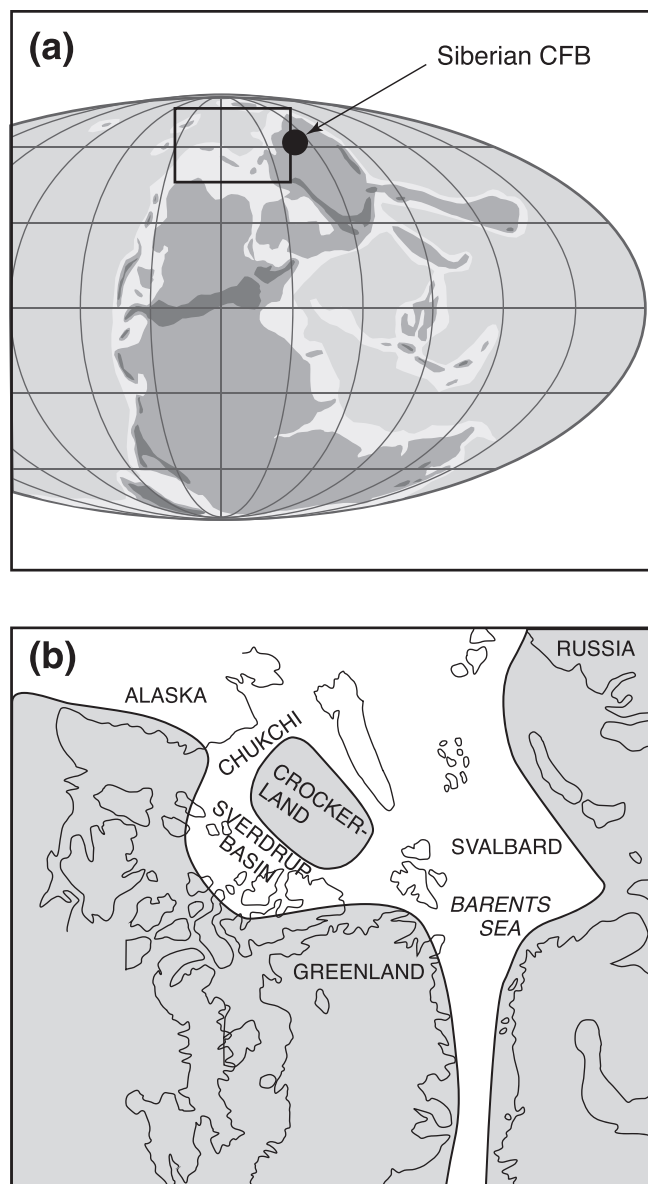


Figure 1. (a) Paleogeography of Late Permian times showing location of Siberian continental flood basalts (CFB) and Spitsbergen in northwest Tethys. (b) Paleogeographic reconstruction of NW Tethys (inset in a) showing location of Spitsbergen in relation to former surrounding land areas.

a palaeolatitude of 40–45°N (Figure 1) in an epicontinental shelf setting on the northern margin of Pangea (Golonka & Ford, 2000; Scotese, 2004). Detailed Hg/TOC, $\delta^{13}\text{C}_{\text{organic}}$ and $\delta^{15}\text{N}$ records for this section were previously published by Grasby et al. (2015a, 2015b, 2020).

2. Samples

The sedimentology and paleontology of the Festningen section has been described in detail by Bond et al. (2015), Grasby et al. (2015a, 2015b), and Wignall et al. (1998), and is summarized in Figure 2. At this location, the boundary between the Permian Kapp Starostin Formation and the overlying latest Permian to Early Triassic Vardebukta Formation corresponds to the LPE horizon (Bond et al., 2015; Grasby et al., 2015a), while the second (earliest Triassic) extinction phase is not manifest at this location nor in other Arctic localities. Bioclastic carbonates are commonly developed in the middle and lower parts of the Kapp Starostin Formation, which reaches around 380 m thickness at this locality (Figure 2). The disappearance of carbonates at around 43 m below the top of the Kapp Starostin Formation (and LPE) marks the Middle Permian (Capitanian) mass extinction level and is associated with elevated Mo/Al and Hg/TOC values (Bond et al., 2015). Above this, the upper 43 m of the Kapp Starostin Formation comprises sandy cherts and pure, spiculitic cherts, with thinner sandstone and shale layers. Above about 58 m, darker shales dominate with occasional chert layers and carbonate concretions (Figure 2). The boundary with the base of the overlying Vardebukta Formation at 90 m corresponds to the LPE, marked by the loss of siliceous sponges and large trace fossils (e.g., *Zoophycos*), followed by the development of mudstone burrowed by small traces for 5 m, and then finely laminated (i.e., unbioturbated) shales (Grasby et al., 2015a, 2015b; Wignall et al., 1998). The onset of an abrupt carbon isotope negative excursion, in which $\delta^{13}\text{C}_{\text{organic}}$ values $> -26\text{‰}$ fall to below -32‰ over a vertical distance of <4 m, occurs in the basal Vardebukta Formation (Grasby et al., 2015a; Figure 2). Grasby et al. (2015b) showed that Hg/TOC ratios increase immediately above the LPE and remain high relative to pre-LPE levels up to about 50 m above the LPE, apparently due to Hg emissions from Siberian volcanism. The Permian-Triassic boundary is placed 6 m above the LPE horizon within the Vardebukta Formation (Grasby et al., 2015a, 2015b; Wignall et al., 2016).

We measured trace element concentrations in 125 sediment samples collected from 31.5 m below, to 24.8 m above the LPE (latest Changhsingian to earliest Griesbachian; Figure 2). Of these samples, 111 (the C-prefix samples in Table S1) are aliquots of the same bulk-rock powders for which $\delta^{13}\text{C}_{\text{organic}}$ and Hg data in Figure 2 were previously reported by Grasby et al. (2015a, 2015b). The 14 FE- prefix samples were collected by Bond et al. (2015) from the same section, extending the profile to -31.5 m below the LPE horizon.

3. Analytical Methods

The FE- prefix samples from the second section from Bond et al. (2015) were obtained as rock fragments approximately 5–10 g weight. Weathered edges were removed before the samples were rinsed with distilled water and dried, then powdered in an agate mill.

Concentrations of trace elements (other than Hg) in all samples were determined by quadrupole ICP-MS at the GeoZentrum Nordbayern, Erlangen. Approximately 0.05 g of powdered sample was accurately weighed

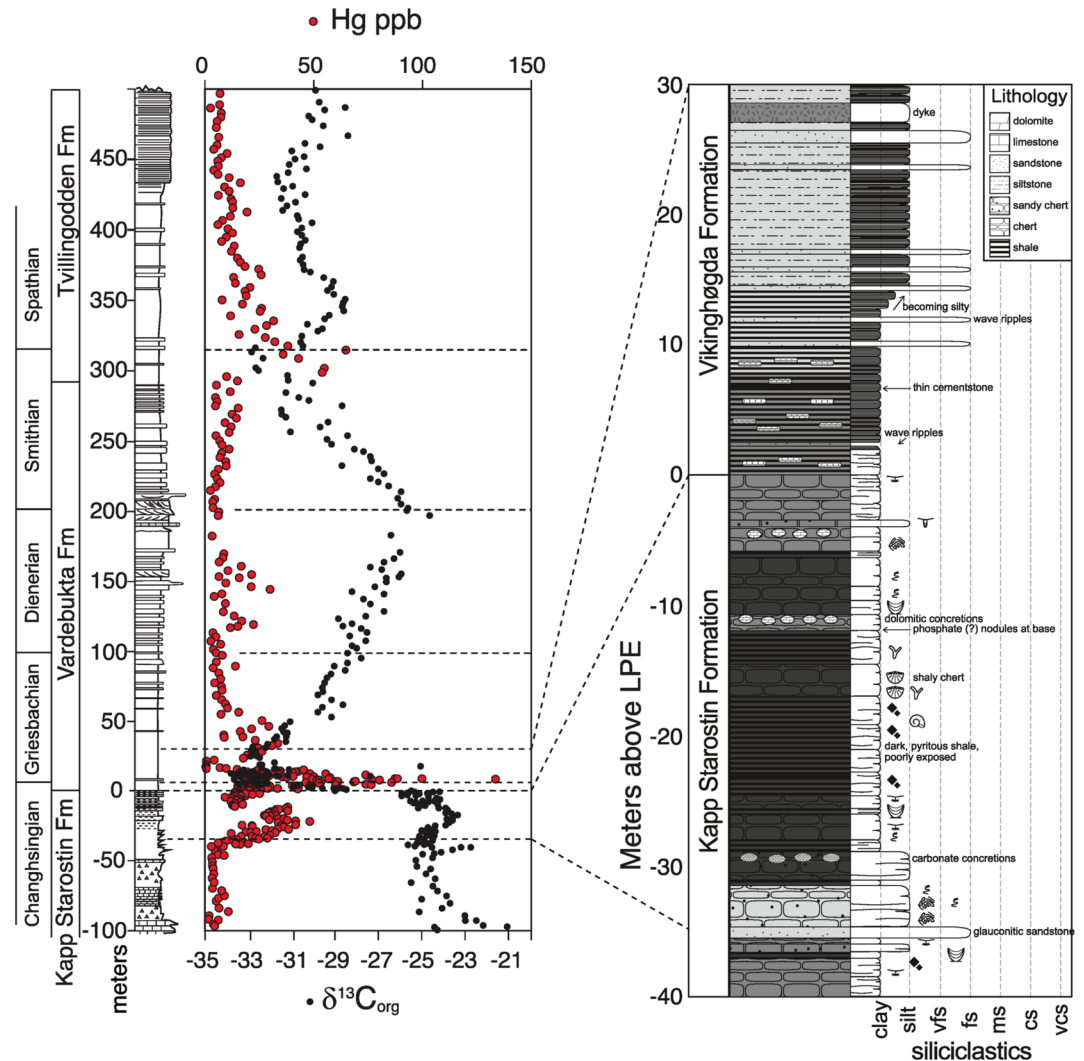


Figure 2. $\delta^{13}\text{C}_{\text{organic}}$ stratigraphy, mercury contents and lithology of Late Permian to Early Triassic sediments from the Festningen section (left panel, from Grasby et al., 2015b), showing sampled interval (right panel). Samples analyzed in this study are from 35 m below to 30 m above the LPE (boundary between the Kapp Starostin and Vikinghogda Formations), which is marked by the onset of the negative $\delta^{13}\text{C}_{\text{organic}}$ excursion and high Hg contents. LPE, Late Permian Extinction.

into a Teflon beaker, and digested in 1 mL 15M HNO_3 and 3 mL 12M HF for 12 h in sealed beakers on a hotplate at 80°C. After cooling, 0.1 mL of HClO_4 was added to the sample, and the solution evaporated to incipient dryness at 120°C. Two milliliter of 15M HNO_3 was added to the sample, and evaporated to near dryness, and this step was repeated twice before increasing the hotplate temperature to 160°C and fuming off excess HClO_4 . The sample was then redissolved in 4 mL 15M HNO_3 and 4 mL H_2O , one drop of 12M HF was added, and the sealed beakers left on a hotplate at 80°C for 12 h. The samples were then placed in an ultrasonic bath for 30 min, before heating at 80°C for another 12 h. At this stage, all samples were completely in solution. The sample solutions were then quantitatively transferred to 250 mL high-density polyethylene bottles and diluted to 200 g with Milli-Q (MQ) water to obtain a final solution of 2% HNO_3 + 0.001 M HF with total dissolved solids of about 250 $\mu\text{g}/\text{mL}$. All reagents used were distilled in Teflon stills and diluted with MQ 18.2 Ohm water.

Trace element measurements were carried out at the GeoZentrum Nordbayern using a Thermo Scientific X-Series 2 quadrupole inductively coupled plasma mass spectrometer. Samples were introduced into the instrument through a Cetac Aridus 2 desolvating nebulizer system in order to enhance sensitivity and re-

duce molecular interferences. An ESI SC-2 DX FAST autosampler was used to reduce washout times between samples. The instrument was tuned using a 5 ppb solution of Be, In, and U; typical sensitivity for ^{238}U was 2×10^6 counts per second for a sample uptake rate of 50 $\mu\text{l}/\text{min}$. The Ce/CeO ratio was $>5,000$, and thus corrections for interferences of oxides of Ba and the light rare-earth elements (REE) on Eu and Gd were unnecessary. Before each measurement session, the instrument was calibrated using multielement solutions covering the relevant concentration range. A mixed Be, In, Rh, and Bi solution (30, 10, 10, 5 ppb) was mixed with the sample online and these elements used as internal standards to correct for instrumental drift. Samples were dissolved and measured in random stratigraphic order. Procedural blanks analyzed during this work were negligible for all elements measured. Accuracy and reproducibility was monitored by repeated analysis of international rock standards (Table S1); for most elements, precision was better than 3% and accuracy better than 5%.

Tellurium and rhenium concentrations were measured on the same sample solutions, after measurement of all other elements in Table S1. The ICP-MS setup was exactly as described previously, but the instrument was tuned to obtain maximum sensitivity for Te (typically $> 125,000$ cps/ppb), and a background in the Te mass range as low as possible (detection limit as determined from 3 sd of repeated blank measurements was generally < 0.3 ppt). The instrument was calibrated using Te standard solutions of 1–50 ppt, and drift was corrected using a mixed Rh-In-Bi internal standard. Tellurium concentrations were determined using 40 ms counting times for both ^{125}Te (7.1%) and ^{126}Te (18.8%) masses, as the contribution of ^{126}Xe (0.09%) at mass 126 was negligible as determined by measurement of ^{129}Xe (26.4%). The Te concentrations determined using both isotopes was generally similar within error (Figure 3), but those obtained from the more precise ^{126}Te measurements are listed in Table S1. Typical precision was between 1% and 5%, and reproducibility as determined by repeated analysis of a 10 ppt solution was better than 7%.

Mercury concentrations in the 14 FE-prefix samples were measured by atomic absorption spectrometry using a DMA-80 direct mercury analyzer (Milestone) from MWS/MLS GmbH. Approximately 0.3 g of sample powder was weighed accurately into a quartz sample holder, and Hg released by thermal decomposition between 650°C and 1,000°C. The Hg released was separated from other volatile components by gold amalgamation, then quantitatively measured by atomic absorption at 253.65 nm. The instrument was calibrated daily using freshly prepared standard solutions with concentrations between 0.05 ng/g and 1,000 ng/g Hg. Blanks were determined at the start, end, and middle of each measurement run and were between 0.03 and 0.1 ng/g. Accuracy was typically better than 3%.

Carbonate contents of the FE- samples were determined by measurement of the CO_2 pressure generated by reaction of 0.5 g sample powder with excess 6 M HCl, with an accuracy of about 3%. The decarbonated residues from this process were thoroughly rinsed with distilled water, then dried and used for the determination of organic carbon concentrations and $\delta^{13}\text{C}_{\text{organic}}$ using gas-source mass spectrometry. Concentrations and isotope compositions of organic carbon of the 14 FE- prefix samples were determined on acid-treated (decarbonated) sample powders, using a Flash EA 2000 elemental analyzer connected online to a ThermoFinnigan Delta V Plus mass spectrometer. All C isotope values in Table S1 are reported in the conventional δ notation in permil relative to Vienna-PDB. Accuracy and reproducibility of the analyses was checked by replicate analyses of laboratory standards calibrated to international standards USGS 40 and 41. Reproducibility was better than $\pm 0.07\text{‰}$ (1σ). Organic carbon concentrations measured in the decarbonated residues were converted to TOC concentrations in the bulk rock using the relationship $\text{TOC} = \text{C content in decarbonated residue} \times (100 - \text{CaCO}_3 \text{ content in } \%) / 100$. However, as the CaCO_3 contents of all but 2 samples were $< 5\%$, the measured organic C contents in the decarbonated samples are close to those of the calculated bulk rock.

4. Results

Concentrations of trace elements for both the C- and FE- prefix samples are listed in Table S1. For the FE- samples, Hg concentrations, $\delta^{13}\text{C}_{\text{organic}}$ values, and bulk-rock CaCO_3 and TOC contents were measured during this study. The Hg, TOC, and $\delta^{13}\text{C}_{\text{organic}}$ data for the C- samples are from Grasby et al. (2015b) using similar methods to our study, except that TOC contents were measured on bulk-rock powder samples using Rock Eval pyrolysis (Grasby et al., 2015b).

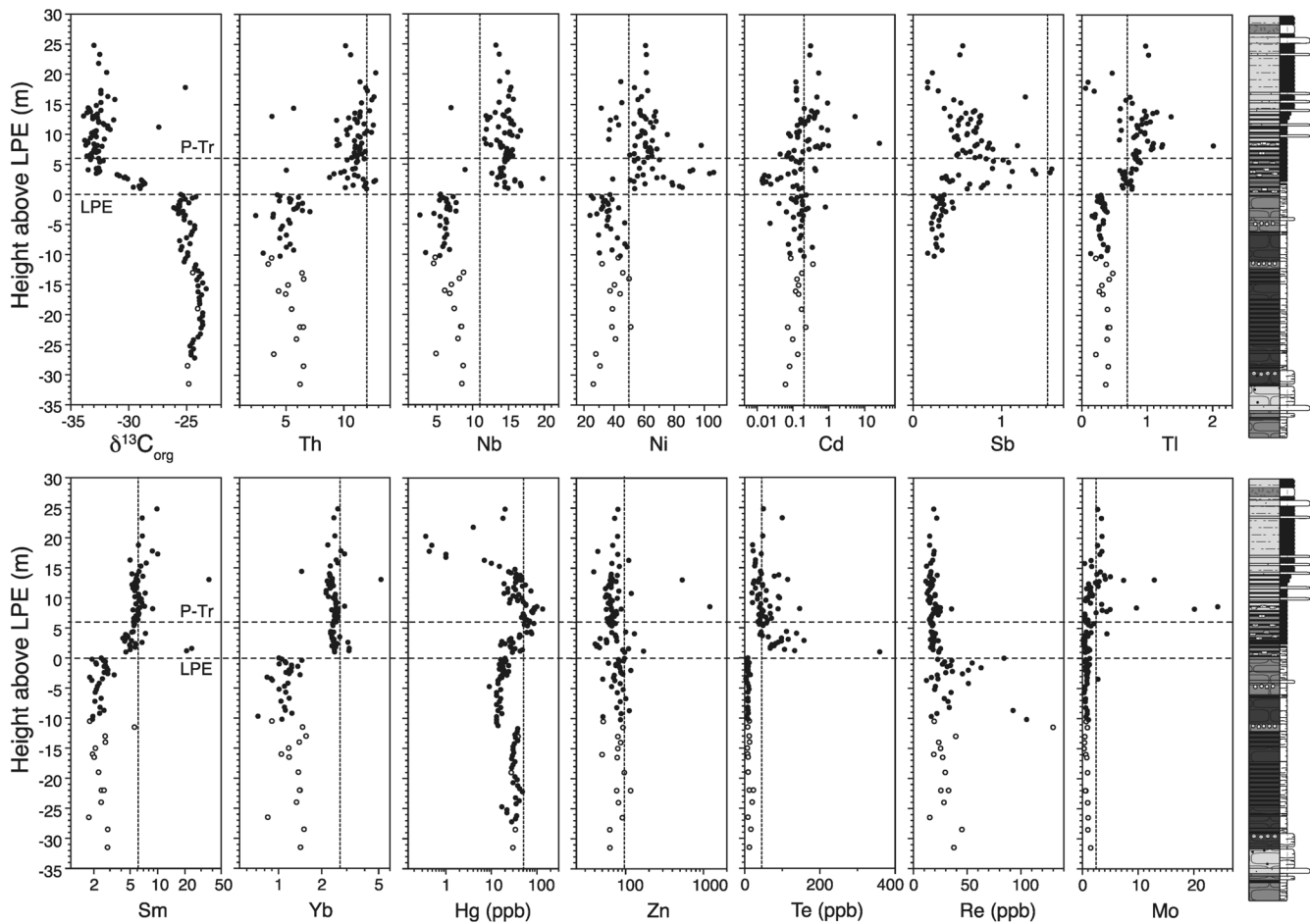


Figure 3. Variations in trace element concentrations, TOC contents and $\delta^{13}\text{C}_{\text{organic}}$ with stratigraphic height (vertical distance above the LPE horizon) for the Spitsbergen sediments. Black symbols are C- prefix samples from Grasby et al. (2015b), white symbols are Fe- prefix samples collected by Bond et al. (2015) from lower in the section. All data are from this study, except for the Hg, TOC, and $\delta^{13}\text{C}_{\text{organic}}$ values for the C- samples (black symbols) which are taken from Grasby et al. (2015b). Elements such as Nb, Th which are contained in the detrital fraction of the sediment and not in biogenic silica, increase by a factor of 2–3 across the LPE, whereas Hg, Te, Cd, Re, Sb show more complex behavior (see text for discussion). Note log scale on x-axis of some diagrams. Concentrations in ppm unless otherwise indicated. Vertical line shows average shale composition (Te from Li, 2000 [Table VI-5a]; Hg from Grasby et al., 2019; all other elements; Turekian & Wedepohl, 1961). LPE, Late Permian Extinction.

CaCO_3 contents of the FE- prefix samples (between -10 and -33 m) are $< 7\%$ for all samples measured, and TOC is below 0.62% . Hg contents of the FE- samples are $10\text{--}40$ ppb and are similar to the Hg concentrations determined by Grasby et al. (2015b) for the same time interval from this section (Figure 3; Figure S1).

Variations in bulk-rock trace element compositions relative to stratigraphic position (vertical distance to the LPE) are shown in Figure 3. Trace elements such as Th, Nb, and Al which are likely contained in the detrital fraction of sediment rather than in carbonate, and also have low concentrations in silica (chert), increase upsection, having lower concentrations in the chert-rich sediments below the LPE, and higher values in the shales and siltstones above the LPE. Both Th and Nb vary by a factor of about 10, and increase by a factor of 2–3 across the LPE. The variation in Sm and Yb is similar, except that two samples immediately above the LPE have anomalously high Sm (Figure 3). The origin of these variations are discussed more fully below.

The concentrations of the chalcophile trace elements Ni and Tl generally also increase upsection (Figure 3) and broadly mirror Th variations, although variations in concentration of these elements are larger (factor of $10\text{--}20$) compared to Th. In contrast, Zn shows no systematic variation upsection, and Cd concentrations show large variations (factor of >100) and do not increase across the LPE, with samples between $+ 3$ and $+ 5$ m having the lowest Cd (Figure 3). Re contents also do not follow Th, but instead are highest in samples

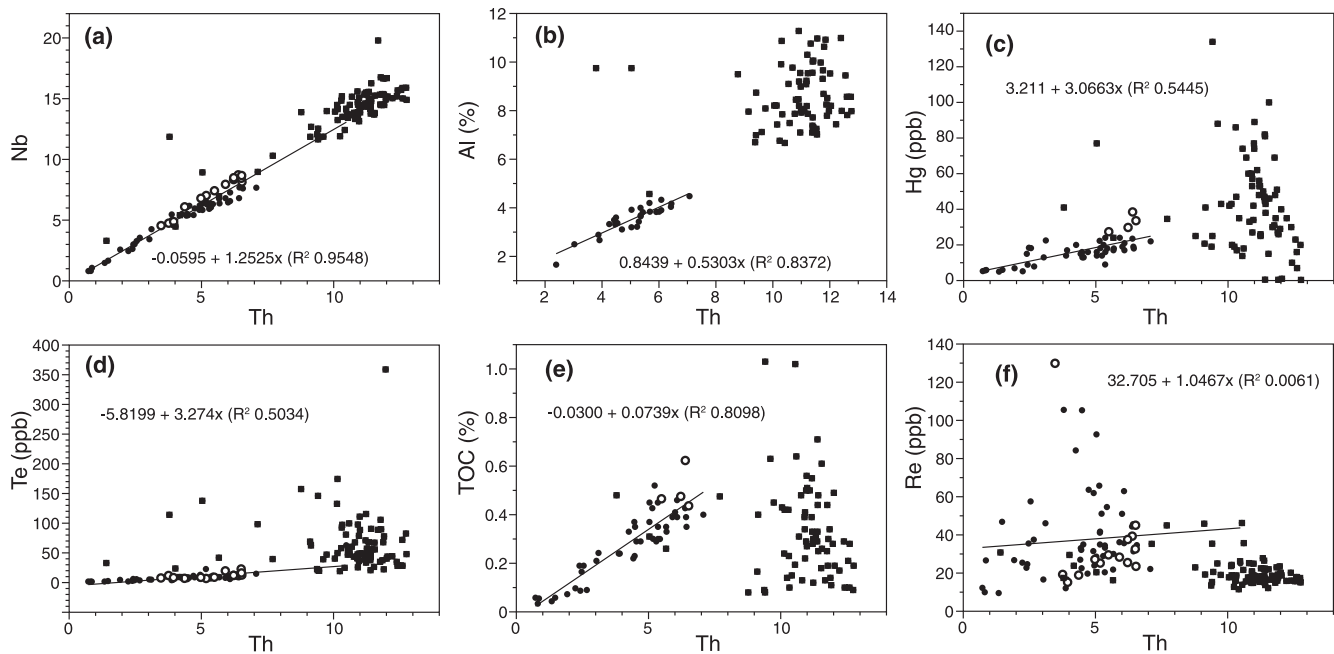


Figure 4. Variation of Nb, Hg, Tl, Te, TOC, and Re with Th. Nb and Th are positively correlated, vary by a factor of 6–7, and increase by a factor of 2–3 across the LPE (circular symbols: pre-LPE, square symbols: post-LPE), due to a decrease in biogenic SiO₂ content, as supported by intercept near origin. Other elements show more complex behavior; Te and Tl are relatively higher in post-LPE sediments than can be explained by variations in SiO₂, whereas Hg and TOC extend to both higher and lower values in post-LPE sediments, and Re is generally higher prior to the LPE. Linear fit in (b–f) for pre-LPE samples. LPE, Late Permian Extinction.

from the 12 m immediately below the LPE, and generally decrease across the LPE. Mo contents are highest in scattered samples between +7 and +13 m, and Sb contents peak at +3–+5 m (Figure 3).

Te contents increase across the LPE, but by a factor of about 10–20 (compared to 2–3 for Th) and the sample with the highest Te concentration (359 ppb) is from the +1 m level directly overlying the LPE (Figure 2). Spitsbergen sediments from below the LPE generally have lower trace element concentrations than average shale (Figure 3), whereas those above the LPE have similar or higher concentrations.

5. Discussion

5.1. Mineralogical and Environmental Controls on Sediment Geochemistry

In order to identify possible enrichments in trace elements due to volcanism, it is necessary to understand the influence of other variables on sediment trace element geochemistry. Some elements are highly sensitive to variations in sediment lithology and mineralogy (e.g., Zr, Hf in zircon, REE and Th in monazite, Nb, Ta in rutile, and chalcophile trace elements may be contained in sulfide). Local environmental effects such as the redox state within the sediment and overlying water column may lead to variations in Mo, U, V, and changes in productivity may influence concentrations of Cd, Zn, and Ni (e.g., Tribovillard et al., 2006). The behavior of many of the trace chalcophile elements (Te, Sb, Tl) is less well known, but can be inferred from their variation with other elements.

Elements that are likely contained in the detrital component of the sediment rather than in biogenic silica or carbonate, for example Th and Nb, vary within the Festningen sediments by a factor of 10–15, and are positively correlated, with correlations passing close to the origin (Figure 4). The concentrations of Th and Nb (as well as Al, Grasby et al., 2015b), generally increase upsection, as the chert content of the sediments decreases (Figure 3). These systematics suggest that the detrital component containing Nb and Th in these sediments has a relatively uniform Nb/Th ratio, and that absolute concentrations of these elements in the sediments vary mainly due to the diluting effect of silica, with chert/quartz containing negligible Th or Nb.

Other trace element variations may be due to mineralogical effects, for example Zr is less well correlated with Th or Nb, likely due to small variations in zircon content, as Zr and Hf are well correlated (not shown). Variations in the carbonate content may influence Sr and U concentrations of sediments, but most of the Spitsbergen sediments have $\text{CaCO}_3 < 5\%$. The REEs have more variable concentrations than Nb or Th (e.g., Ce varies by a factor of about 60) and show more complex behavior, with at least two distinct REE-enriched phases. One has relatively high middle REE (e.g., Sm) and Y contents, which is responsible for high Sm and Sm/Yb in samples C556636 and C556638 at 2–3 m above the LPE, and sample FE74 at –12 m (Figure 3). This phase is likely phosphate, which can have high Sm/Yb ratios.

Other trace elements are sensitive to environmental factors, for example Mo, V, and U concentrations in sediments are known to be sensitive to the local redox state within the sediment and overlying water column, and Ni, Zn, Cu vary with productivity (e.g., Tribovillard et al., 2006). Grasby et al. (2015b) and Bond et al. (2015) showed that in the Spitsbergen section, Mo concentrations and Mo/Al ratios increase abruptly at the onset of the Capitanian Crisis at 43 m below the LPE and also at the Smithian-Spathian boundary, known to be marked in many sedimentary sections by an increase in the extent and intensity of oxygen depletion. Both our new data, and the Mo/Al ratios determined by Grasby et al. (2015b) and Bond et al. (2015) for the same samples, show that there is no large change in relative Mo concentrations due to local anoxia across the LPE at Spitsbergen, but instead scattered higher Mo values 7–9 m above the LPE and within the earliest Triassic (Figure 3).

The influence of these factors on the chalcophile element contents of the Spitsbergen sediments is discussed below.

5.2. Chalcophile Trace Elements Ni, Zn, Cd, Sb, Te, Re, and Tl

As discussed above, variations in the chert (silica) content of the sediments have an important control on the concentrations of elements that are not contained in silica. The increase in concentration of many trace elements at the level of the LPE corresponds to the disappearance of biogenic silica at this level. In order to remove this, silica-dilution effect, we have normalized chalcophile element concentrations to Th, an element not contained in silica or carbonate, and which is also not enriched in volcanic gases (e.g., Zelenski et al., 2014). None of the samples have anomalously high Th, high REE, and low Nb/Th which would indicate the presence of Th-rich monazite (Figure 4).

Hg, Tl, Re, and TOC variations are not simply due to silica dilution, as these elements behave differently from Th. For example, sediments from above the LPE (mainly those with Th > 8 ppm in Figure 4) extend to both higher and lower Hg/Th compared to pre-LPE sediments, whereas Tl/Th is generally higher above the LPE, and Re/Th and TOC/Th are significantly lower (Figures 4 and 5).

High Ni concentrations in P-Tr boundary sediments have been attributed to volcanism (Rampino et al., 2017; Rothman et al., 2014). Although Ni concentrations increase across the LPE at Festningen (Figure 3), this is likely due to the silica-dilution effect. Rampino et al. (2017) reported Ni concentrations, whereas Rothman et al. (2014) calculated carbonate-free Ni concentrations for the Meishan section and found Ni enrichment in LPE sediments. At Festningen, there is no significant increase in Ni/Th across the LPE (Figure 5). Instead, most samples with Ni/Th > 10 are from below –10 m in the latest Permian (Figure 5). If normalized Ni enrichments in other P-Tr sections are due to volcanism, our data show that these are not globally distributed. The Sb/Th ratios also show no significant change across the LPE and P-Tr, except that the four samples with highest Sb/Th are located between +3 and +5 m (Figure 5), where Hg/TOC values are highest.

Re/Th values are highest in the interval –8 to –12 m below the LPE, and Re/Th decreases across the LPE (Figure 4). The Re/Th variations do not resemble those of any other trace elements. Our analyses of sediments from other locations have shown that the carbonate fraction of sediments can contain significant Re, but most Spitsbergen sediments have $\text{CaCO}_3 < 5\%$, and there is no relationship between Re/Th and CaCO_3 contents. The origin of the variations in Re/Th in the Spitsbergen sediments is therefore unclear, but assuming that Hg/TOC variations (Figure 5) result from volcanic input of Hg (Grasby et al., 2015a), the variation in Re/Th is inconsistent with volcanic input of Re at or following the LPE.

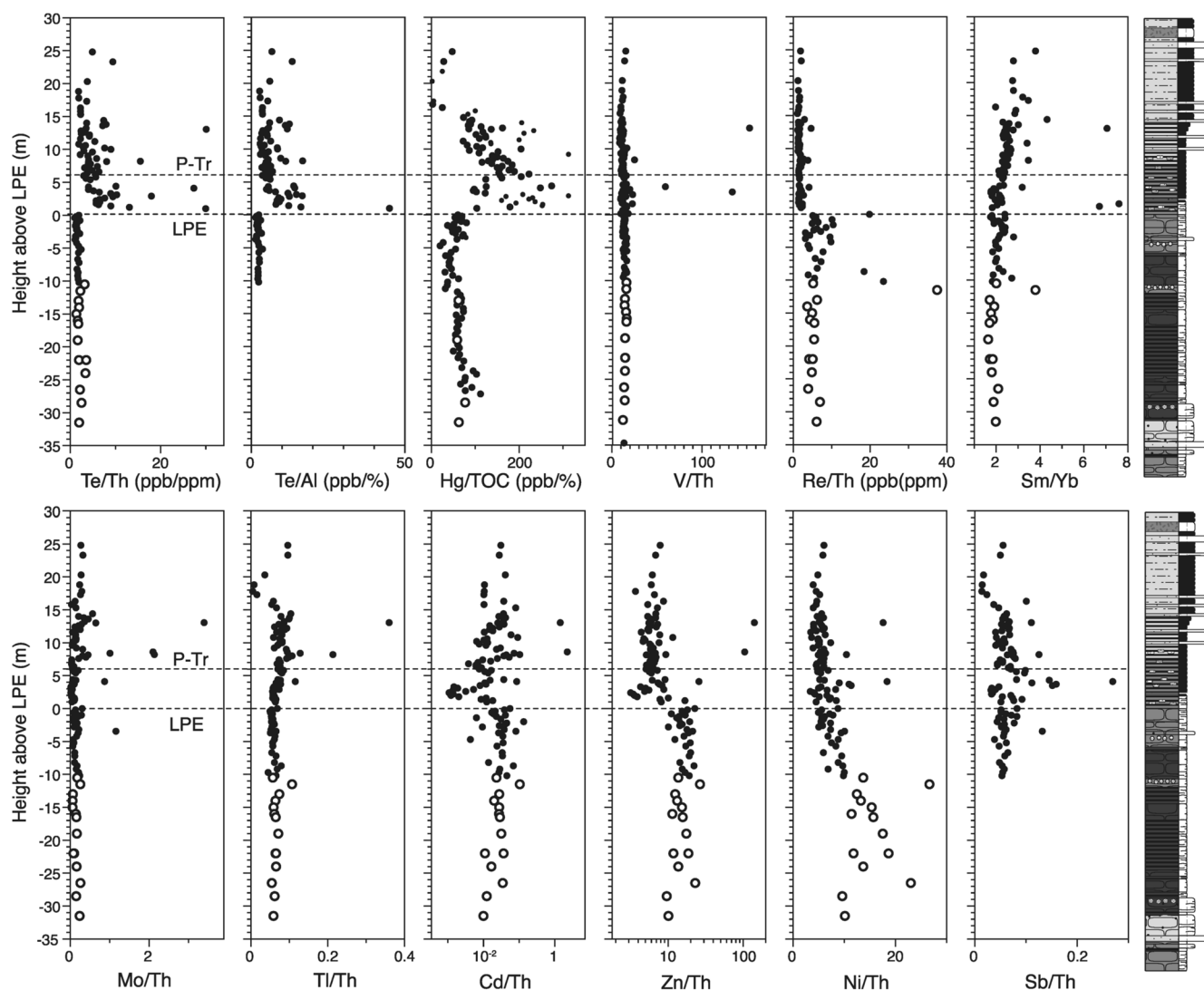


Figure 5. Variations in trace element concentrations normalized to Th to remove SiO₂ dilution effects. Shown for comparison is Hg/TOC (values for the C- samples are from Grasby et al. (2015b); samples with <0.2% TOC are shown as smaller symbols). Ni/Th and Zn/Th decrease across the LPE, likely due to productivity effects reflected also in Cd/Th. Re/Th also decreases across the LPE. The similarity in Tl/Th and Mo/Th suggest that Tl variations partly reflect differences in redox conditions. The Te/Th and Hg/TOC profiles are very similar, suggesting that Te variations reflect volcanic input of Te, first beginning at the LPE (see text for discussion). Correlation coefficients for these ratios are shown in Figure 6. LPE, Late Permian Extinction.

Cd/Th decreases across the LPE, the lowest values are at +2–+3 m above the LPE (Figure 5). Although Cd is enriched in volcanic gases (Symonds et al., 1987; Zelenski et al., 2013), its concentration in marine sediments is also sensitive to variations in productivity (e.g., Tribovillard et al., 2006). Zn/Th follows Cd/Th (Figures 5 and 6), therefore in the Spitsbergen sediments, Zn likely varies due to productivity control.

Tl/Th follows Mo/Th (Figure 6), with higher values of both ratios in four samples between +4 and +13 m height (Figure 5), suggesting that small variations in local redox conditions control Tl (e.g., Them et al., 2018), rather than volcanic input of Tl.

5.3. Te Concentrations and the Te/Th Ratio as a Proxy for Volcanism

Te concentrations vary between 1.8 and 359 ppb (factor of 124), an order of magnitude greater than the total variation in Th or Nb. Below the LPE, Te concentrations are <15 ppb, the highest value is in sample C556635 immediately above the LPE at +1 m. Most samples from the sediments between the LPE and the

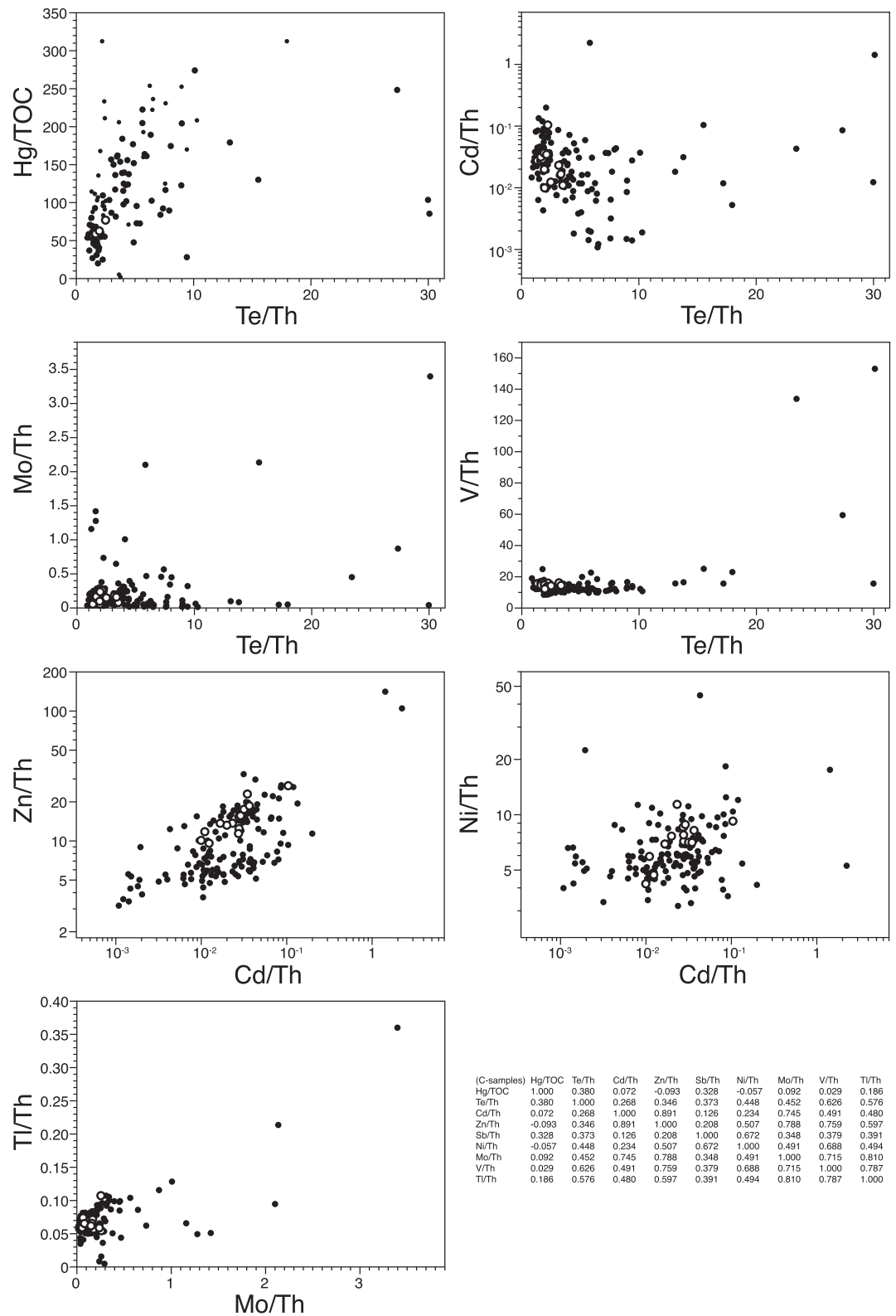


Figure 6. Hg/TOC and Th-normalized concentrations of Ni, Co, Cd, Zn, Sb, Ni, and Te, showing positive correlation between Te/Th and Hg/TOC, and similar behavior of the trace chalcophile element pairs Cd-Zn, Cd-Ni, and Mo-Tl, consistent with redox control on the chalcophile element Tl, and productivity control on Zn and Cd (see text). Inset shows correlation matrix for C- prefix samples (black symbols) for trace element ratios discussed in the text.

P-Tr boundary at +6 m have higher Te contents than average shale (Figure 3), and average upper continental crust (3 ppb).

Te contents generally increase upsection, similar to Th, consistent with partial control by silica dilution. However, the approximately factor of 10 increase in Te content across the LPE is greater than that of Th. In addition, unlike Th and Nb, Te contents and Te/Th ratios progressively decrease above the LPE (Figures 2 and 4). The Te/Th ratios vary by factor >20, and with two exceptions, the samples with Te/Th > 10 are all from the 0–5 m interval immediately above the LPE, and at the same level as the highest Hg/TOC ratios in the same samples (Figure 4). The profiles for Te/Th and Te/Al are similar (Figure 5), although the Te/Al variations suggest that the two higher Te/Th values at +4.1 (C556651) and +13.05 m (C556695) are likely due to low Th contents, rather than especially high Te. These two samples also have relatively high Mo/Th, Tl/Th, Cd/Th, and Zn/Th. Compared to Al, Th contents may be more sensitive in general to the presence of accessory phases, for example, monazite. Normalizing to Th however has the advantage that both elements (together with the other trace elements) can be measured rapidly on the same sample dissolutions using the same analytical method.

The high Te contents in the Festningen sediments immediately above the LPE horizon are not easily explained by mineralogical or lithological effects. Te can be hosted in certain mineral phases, for example, hydrothermal pyrite may have Te contents of several hundred ppm (e.g., Keith et al., 2018). Although pyrite framboids are present in some of the Spitsbergen sediments, Te concentrations and Te/Th ratios are unrelated to the abundance of pyrite in these sediments. The pyrite-rich shales at about –20 m below the LPE (Figure 2) have low Te concentrations similar to other pre-LPE sediments (Figure 3). Bond et al. (2015) reported the size and abundance of pyrite framboids in the FE- samples, but although sample FE77 has approximately 30 times by volume the pyrite content of FE80 (Bond et al., 2015), Te concentrations and Te/Th ratios of these two samples are similar (Figure 4).

Tellurium is also highly enriched in sedimentary Fe-Mn nodules (Hein et al., 2003) and Fe-Mn oxyhydroxide precipitates, but sediments with a significant hydrogenous Fe-Mn component should also have high Mo, Tl, and REE contents (Hein et al., 2003), and there is no clear relationship between Mo/Th or Tl/Th and Te/Th as would be expected if Te was concentrated in Fe-Mn precipitates (Figures 4 and 5). Two samples immediately above the LPE at between 0 and + 2 m height have anomalously high concentrations of the middle REEs and high Sm/Yb ratios (Figures 3 and 5), likely in a phosphate phase as discussed above. In contrast, Te/Th is elevated relative to pre-LPE values throughout the 0 to +10 m overlying the LPE, indicating that the carrier phase of Sm is not also enriched in Te. Although Te can exist in different oxidation states (Te^{IV} , Te^{VI}), the Te/Th ratios of the Spitsbergen sediments do not vary with changes in degree of oxidation as inferred from Mo/Th or V/Th (Figures 5 and 6). Nor does Te/Th vary with variations in productivity as inferred from Cd/Th (Figure 6).

Instead, the variations in Te/Th are very similar to those of Hg/TOC as determined by Grasby et al. (2015b) in the same samples (Figure 5). Hg/TOC ratios are positively correlated with Te/Th (Figure 6), whereas Hg/TOC correlates less well with Mo/Th, Zn/Th, V/Th and Cd/Th (correlation coefficients in Figure 6). Although there are also significant correlations of Te/Th with some of the other trace element ratios in Figure 6, these arise partly from the use of Th in the denominator of both ratios, and correlations are controlled by a few samples with low Th contents, for example, at +5 m and +13 m (Figures 3 and 5).

On the basis of the Te/Th-Hg/TOC correlation and the similarity in the depth profiles of Te/Th and Hg/TOC (Figure 5), we interpret the higher Te and Te/Th immediately above the LPE to be volcanic in origin. Te/Th ratios of the Spitsbergen sediments vary by a factor of about 30, from 0.98 to 30.1. Te/Th increases by a factor of about 10–20 across the LPE, which is greater than the variation in Hg/TOC (about a factor of 4, see also Figure S2), consistent with the high enrichment factor for Te in volcanic gas relative to erupted lavas (10^6 – 10^7 ; Zelenski et al., 2014). Little is known about the speciation of Te in volcanic gas, but it is apparently present as a highly volatile form possibly as Te halide (F, Cl) or hydride (Moune et al., 2006; Symonds & Reed, 1993), which is deposited only in the coolest parts of volcanic gas collection equipment (Zelenski et al., 2013, 2014). The atmospheric residence time of volcanic Te is unknown, although our results imply that volcanic Te can be widely distributed over distances of several 1,000 km during flood basalt events.

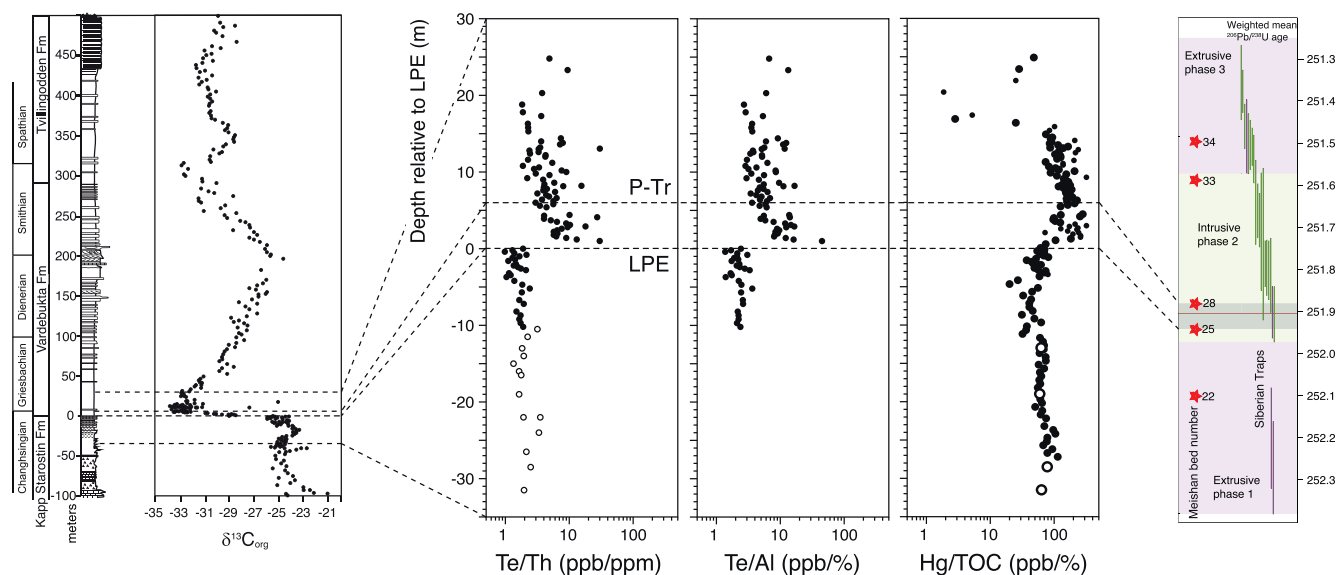


Figure 7. Correlation of the Spitsbergen P-Tr section with dated Siberian intrusive and extrusive magmatic rocks, on the basis of absolute ages for sediments from the Meishan P-Tr section (U-Pb ages from Burgess et al., 2017). In Spitsbergen, the LPE and the P-Tr boundary can be correlated with bed numbers 25–28 in the Meishan GSSP, representing a period of less than 110 kyr. Although the sediments analyzed in our study likely represent a small part of the time period during which Siberian volcanism was apparently active, Hg/TOC and Te/Th (and Te/Al shown for comparison) suggest there was no significant volcanic input to Spitsbergen sediments prior to the LPE, and that the most intense phase of Siberian volcanism initiated at the LPE (the period corresponding to mainly intrusive volcanism according to Burgess et al., 2017), and continued across the Changhsingian-Griesbachian boundary at a lower rate. Alternatively, the LPE corresponds to the start of intrusive Siberian magmatism (Burgess et al., 2017), releasing Hg, Te, and light carbon from intruded sediments. The Hg/TOC and $\delta^{13}\text{C}_{\text{organic}}$ values for the C- samples are from Grasby et al. (2015b), the diagram showing U-Pb ages for Meishan sediments (labeled by bed number) and Siberian magmatic rocks is modified from Burgess et al. (2017). Note same log scale for Te/Th, Te/Al, and Hg/TOC. The Hg/TOC, Al, and $\delta^{13}\text{C}_{\text{organic}}$ data for the C- samples are from Grasby et al. (2015b), from which left-hand panel of the diagram was adapted. Hg/TOC ratios for samples with TOC values < 0.2% are shown as smaller symbols. LPE, Late Permian Extinction.

Although not measured in this study, selenium may behave similarly to Te due to its volatility and similarly high enrichment factor in volcanic gas (Symonds et al., 1987; Zelenski et al., 2014).

5.4. Implications for the Role of Siberian Volcanism in Late Permian-Early Triassic Environmental Change and Contemporaneous Extinction

The increase in Te/Th and Hg/TOC at the level of the negative $\delta^{13}\text{C}_{\text{organic}}$ excursion at the LPE (Figure 7), implies onset of abrupt and intense emissions from Siberian volcanism at that time. Assuming a direct link between Te/Th and Hg/TOC and the volume of extrusive volcanism, would imply that the most intense period of Siberian volcanism occurred between the LPE and the P-Tr boundary at approximately +6 m (a period of 60–108 kyr; Burgess et al., 2017), and continued at decreasing rate into the Early Triassic, possibly explaining the extended period of global oceanic anoxia (Grasby et al., 2013a, 2013b; Wignall et al., 2016) and delayed recovery of fauna and bioproductivity during the Early Triassic (Grasby et al., 2020). Alternatively, the decreasing, but elevated Te/Th and Hg/TOC values in the Early Triassic could reflect remobilization and deposition of Hg and Te from earlier volcanism, although it is unlikely that Hg and Te would behave so similarly as reflected in the Hg/TOC and Te/Th variations during this period, and would imply an unreasonably short timeframe for Siberian volcanism.

Estimates of the timing of Siberian extrusive volcanism relative to the LPE and the associated carbon isotope excursion, and the P-Tr boundary based on Te/Th and Hg/TOC are broadly consistent with available high-precision U-Pb zircon ages of both Siberian volcanism and P-Tr sediment sections, but would suggest a shorter timescale for the main phase of volcanism (Figure 7). According to U-Pb ages, approximately 60%–70% (an approximately 4-km thick section) of the Siberian lava pile was erupted within about 300 kyr, ending at the LPE (Phase 1 of Burgess et al., 2017, see Figure 7), at which time massive intrusion of sills is

inferred to have occurred (Phase 2). Thereafter, extrusive volcanism continued at a lower rate into the Early Triassic (extrusive Phase 3 of Burgess et al., 2017; see Figure 7), until about 251.3 Ma.

If Te and Hg are not widely released or distributed during intrusive magmatism, and Te/Th variations reflect the intensity of extrusive magmatism, then Te/Th and Hg/TOC in Spitsbergen sediments would imply that the main phase of extrusive Siberian volcanism initiated abruptly at the LPE at 251.9 Ma, rather than prior to the LPE (at least during the few 100 ky likely recorded in our samples from below the LPE). The Te and Hg records in Spitsbergen sediments would therefore suggest a much shorter timeframe for extrusive Siberian volcanism compared to U-Pb ages (Figure 7).

Burgess et al. (2017) correlated the carbon isotope excursion at the LPE with the start of intense intrusive magmatism in Siberia. An alternative explanation for the enrichment in Hg and Te at the level of the LPE is therefore that these elements were sourced from sediments in the Siberian Basin, including coals which may have high Te contents (e.g., Bullock et al., 2019), and widely distributed during explosive gas (CO₂, CH₄) release during metamorphism (Svensen et al., 2009). This scenario would explain the enrichment of Hg and Te and carbon with low δ¹³C at the level of the LPE, associated with abrupt warming of up to 7°C (Sun et al., 2012) and widespread marine anoxia. Further analyses of sediments extending the geochemical record to older and younger ages, to cover the entire timespan of Siberian U-Pb ages (approximately 0.7–1.1 My; Figure 7) are required to determine whether Te and Hg are magmatic or metamorphic in origin.

6. Conclusions

Te concentrations in sediments, and the Te/Th ratio may be a useful proxy for the intensity of volcanism in the past, allowing the records of volcanism, biotic changes, and paleoenvironment to be examined in the same sedimentary sections. In contrast, variations in other chalcophile trace elements, including Ni, Zn, Sb, Re, Tl, and Cd in Spitsbergen P-Tr sediments, do not vary due to volcanic input, but rather reflect changes in local redox conditions and paleoproductivity and sediment mineralogy. Te/Th ratios in Spitsbergen sediments imply that Siberian volcanism initiated at the LPE, and that most magma was emplaced within a short (a few 100 ky) period between the LPE and the P-Tr boundary, continuing at a lower rate into the earliest Griesbachian. Further analyses of other P-Tr sections worldwide will determine whether high Te/Th ratios are a widespread feature of the P-Tr crisis. Our study shows the potential of Te as an additional LIP-mark (cf. Grasby et al., 2019) which could be applied to the sedimentary archives of other mass extinction events associated with LIP magmatism.

Data Availability Statement

Trace element and carbon isotope data produced during this study will be archived at PANGAEA Data Archiving and Publication (<https://doi.org/10.1594/PANGAEA.923639>). An electronic copy of this data file is provided as Supporting Information.

Acknowledgments

This work was funded by the Deutsche Forschungsgemeinschaft (DFG) through grant RE 3020/10-1 as part of the DFG Forschergruppe TER-SANE (FOR 2332). David P. G. Bond acknowledges funding from the Natural Environment Research Council (grant numbers NE/J01799X/1 and NE/J015817/1). We thank Michael Joachimski for the organic carbon concentration and δ¹³C_{organic} measurements of the Fe-samples, M. Joachimski and W. Kiessling for discussions, and the three reviewers for their helpful comments. Open access funding enabled and organized by Projekt DEAL.

References

- Algeo, T. J., & Twitchett, R. J. (2010). Anomalous Early Triassic sedimentary fluxes due to elevated weathering rates and the biological consequences. *Geology*, 38, 1023–1026.
- Beauchamp, B., & Grasby, S. E. (2012). Permian lysocline shoaling and ocean acidification along NW Pangea led to carbonate eradication and chert expansion. *Palaeogeography, Palaeoclimatology, Palaeoecology*, 350–352, 73–90.
- Bond, D. P. G., & Grasby, S. E. (2017). On the causes of mass extinctions. *Palaeogeography, Palaeoclimatology, Palaeoecology*, 478, 3–29.
- Bond, D. P. G., & Wignall, P. B. (2014). Large igneous provinces and mass extinctions: An update. In G. Keller, & A. C. Kerr (Eds.), *Volcanism, impacts, and mass extinctions: Causes and effects* (Vol. 505, (29–55)). Geological Society of America Special Paper. [https://doi.org/10.1130/2014.2505\(02\)](https://doi.org/10.1130/2014.2505(02))
- Bond, D. P. G., Wignall, P. B., Joachimski, M. M., Sun, Y., Savov, I., Grasby, S. E., et al. (2015). An abrupt extinction in the Middle Permian (Capitanian) of the Boreal Realm (Spitsbergen) and its link to anoxia and acidification. *The Geological Society of America Bulletin*, 127, 1411–1421.
- Bowring, S. A., Erwin, S. A., Jin, Y. G., Martin, M. W., Davidek, K., & Wang, W. (1998). U/Pb zircon geochronology and tempo of the End-Permian mass extinction. *Science*, 280, 1039–1045.
- Bullock, L. A., Parnell, J., Feldmann, J., Armstrong, J. G., Henn, A. S., Mesko, M. F., et al. (2019). Selenium and tellurium concentrations of Carboniferous British coals. *Geological Journal*, 54, 1401–1412.

- Burgess, S. D., & Bowring, S. A. (2015). High precision geochronology confirms voluminous magmatism before, during and after Earth's most severe extinction. *Science Advances*, *1*, e1500470.
- Burgess, S. D., Bowring, S., & Shen, S. (2014). High-precision timeline for Earth's most severe extinction. *Proceedings of the National Academy of Sciences*, *111*, 3316–3321.
- Burgess, S. D., Muirhead, J. D., & Bowring, S. A. (2017). Initial pulse of Siberian Traps sills as the trigger of the end-Permian mass extinction. *Nature Communications*, *8*, 164.
- Calvert, S. E., & Pedersen, T. F. (1996). Sedimentary geochemistry of manganese: Implications for the environment of formation of manganeseiferous black shales. *Economic Geology*, *91*, 36–47.
- Charbonnier, G., Adatte, T., Föllmi, K. B., & Suan, G. (2020). Effect of intense weathering and post-depositional degradation of organic matter on Hg/TOC proxy in organic-rich sediments and its implications for deep-time investigations. *Geochemistry, Geophysics, Geosystems*, *21*, e2019GC008707. <https://doi.org/10.1029/2019GC008707>.
- Clarkson, M. O., Kasemann, S. A., Wood, R., Lenton, T. M., Daines, S., Richoz, S., et al. (2015). Ocean acidification and the Permo-Triassic mass extinction. *Science*, *348*, 229–232.
- Erwin, D. H. (1994). The Permo-Triassic extinction. *Nature*, *367*, 231–236.
- Fantasia, A., Adatte, T., Spangenberg, J. E., Font, E., Duarte, L. V., & Föllmi, K. B. (2019). Global versus local processes during the Pliensbachian-Toarcian transition at the Peniche GSSP, Portugal: A multi-proxy record. *Earth-Science Reviews*, *198*, 102932.
- Golonka, J., & Ford, D. (2000). Pangean (Late Carboniferous–Middle Jurassic) paleoenvironment and lithofacies. *Palaeogeography, Palaeoclimatology, Palaeoecology*, *161*, 1–34.
- Grasby, S. E., Beauchamp, B., Bond, D. P. G., Wignall, P. B., & Sanei, H. (2015b). Mercury anomalies associated with three extinction events (Capitanian Crisis, Latest Permian Extinction and the Smithian/Spathian Extinction) in NW Pangea. *Geological Magazine*, *153*, 285–297.
- Grasby, S. E., Beauchamp, B., Bond, D. P. G., Wignall, P. B., Talavera, C., Galloway, J. M., Piepjohn, K., et al. (2015a). Progressive environmental deterioration in NW Pangea leading to the Latest Permian Extinction. *The Geological Society of America Bulletin*, *127*, 1331–1347. <https://doi.org/10.1130/B31197.1>
- Grasby, S. E., Beauchamp, B., Embry, A., & Sanei, H. (2013a). Recurrent Early Triassic anoxia. *Geology*, *41*, 175–178.
- Grasby, S. E., Knies, J., Beauchamp, B., Wignall, P., & Sun, Y. (2020). Global warming leads to Early Triassic nutrient stress across northern Pangea. *The Geological Society of America Bulletin*, *132*, 943–954. <https://doi.org/10.1130/B32036.1>
- Grasby, S. E., Sanei, H., & Beauchamp, B. (2011). Catastrophic dispersion of coal fly ash into oceans during the latest Permian extinction. *Nature Geoscience*, *4*, 104–107.
- Grasby, S. E., Sanei, H., Beauchamp, B., & Chen, Z. (2013b). Mercury deposition through the Permo-Triassic Biotic Crisis. *Chemical Geology*, *351*, 209–216.
- Grasby, S. E., Shen, W., Yin, R., Gleason, J. D., Blum, J. D., Lepak, R. F., et al. (2016). Isotopic signatures of mercury contamination in latest Permian oceans. *Geology*, *45*, 55–58.
- Grasby, S. E., Them, T. R., Chen, Z., Yin, R., & Ardakani, O. H. (2019). Mercury as a proxy for volcanic emissions in the geologic record. *Earth-Science Reviews*, 102880. <https://doi.org/10.1016/j.earscirev.2019.102880>
- Hein, J. R., Koschinsky, A., & Halliday, A. N. (2003). Global occurrence of tellurium-rich ferromanganese crusts and a model for the enrichment of tellurium. *Geochimica et Cosmochimica Acta*, *67*, 1117–1127.
- Joachimski, M. M., Lai, X., Shen, S., Jiang, H., Luo, G., Chen, B., et al. (2012). Climate warming in the latest Permian and the Permian-Triassic mass extinction. *Geology*, *40*, 195–198.
- Keith, M., Smith, D. J., Jenkin, G. R. T., Holwell, D. A., & Dye, M. D. (2018). A review of Te and Se systematics in hydrothermal pyrite from precious metal deposits: Insights into ore-forming processes. *Ore Geology Reviews*, *96*, 269–282.
- Korte, C., Pande, P., Kalia, P., Kozur, H. W., Joachimski, M. M., & Oberhänsli, H. (2010). Massive volcanism at the Permian-Triassic boundary and its impact on the isotopic composition of the ocean and atmosphere. *Journal of Asian Earth Sciences*, *37*, 293–311.
- Li, Y.-H. (2000). *A compendium of geochemistry: From solar nebula to the human brain* (p.). Princeton and Oxford: Princeton University Press.
- Liu, S.-A., Wu, H., Shen, S.-z., Jiang, G., Zhang, S., Lv, Y., et al. (2017). Zinc isotope evidence for intensive magmatism immediately before the end-Permian mass extinction. *Geology*, *45*, 343–346.
- Moune, S., Gauthier, P.-J., Gislason, S. R., & Sigmasson, O. (2006). Trace element degassing and enrichment in the eruptive phase of the 2000 eruption of Hekla volcano, Iceland. *Geochimica et Cosmochimica Acta*, *70*, 461–479.
- Percival, L. M. E., Ruhl, M., Hesselbo, S. P., Jenkyns, H. C., Mather, T. A., & Whiteside, J. H. (2017). Mercury evidence for pulsed volcanism during the end-Triassic mass extinction. *Proceedings of the National Academy of Sciences*, *114*, 7929–7934.
- Percival, L. M. E., Witt, M. L. I., Mather, T. A., Hermoso, M., Jenkyns, H. C., Hesselbo, S. P., et al. (2015). Globally enhanced mercury deposition during the end-Pliensbachian extinction and Toarcian OAE: A link to the Karoo-Ferrar Large Igneous Province. *Earth and Planetary Science Letters*, *428*, 267–280.
- Rampino, M. R., Rodriguez, S., Baransky, E., & Cai, Y. (2017). Global nickel anomaly links Siberian Traps eruptions and the latest Permian mass extinction. *Scientific Reports*, *7*, 12416.
- Reichow, M. K., et al. (2009). The timing and extent of the eruption of the Siberian Traps large igneous province: Implications for the end-Permian environmental crisis. *Earth and Planetary Science Letters*, *277*, 9–20.
- Renne, P. R., Zichao, Z., Richards, M. A., Black, M. T., & Basu, A. R. (1995). Synchrony and causal relations between Permian-Triassic boundary crises and Siberian flood volcanism. *Science*, *269*, 1413–1416.
- Rothman, D. H., Fournier, G. P., French, K. L., Alm, E. J., Boyle, E. A., Cao, C., & Summons, R. E. (2014). Methanogenic burst in the end-Permian carbon cycle. *Proceedings of the National Academy of Sciences*, *111*, 5462–5467.
- Sanei, H., Grasby, S. E., & Beauchamp, B. (2012). Latest Permian mercury anomalies. *Geology*, *40*, 63–66.
- Saunders, A., & Reichow, M. (2009). The Siberian Traps and the end-Permian mass extinction: A critical review. *Chinese Science Bulletin*, *54*, 20–37.
- Scotese, C. R. (2004). A continental drift flipbook. *The Journal of Geology*, *112*, 729–741.
- Shen, J., Algeo, T. J., Chen, J., Planavsky, N. J., Feng, Q., Yu, J., & Liu, J. (2019a). Mercury in marine Ordovician/Silurian boundary sections of South China is sulfide-hosted and non-volcanic in origin. *Earth and Planetary Science Letters*, *511*, 130–140.
- Song, H. J., Wignall, P. B., Tong, J. N., & Yin, H. F. (2013). Two pulses of extinction during the Permian-Triassic crisis. *Nature Geoscience*, *6*, 52–56.
- Sun, Y., Joachimski, M. M., Wignall, P. B., Yan, C., Jiang, H., Wang, L., & Lai, X. (2012). Lethally hot temperatures during the Early Triassic. *Science*, *338*, 366–370.

- Svensen, H., Planke, S., Polozov, A. G., Schmidbauer, N., Corfu, F., Podladchikov, Y. Y., & Jamtveit, B. (2009). Siberian gas venting and the end-Permian environmental crisis. *Earth and Planetary Science Letters*, *227*, 490–500.
- Symonds, R. B., & Reed, M. H. (1993). Calculation of multicomponent chemical equilibria in gas-solid-liquid systems: Calculation methods, thermochemical data, and applications to studies of high-temperature volcanic gases with examples from Mount St. Helens. *American Journal of Science*, *293*, 758–864.
- Symonds, R. B., Rose, W. I., Reed, M. H., Lichte, F. E., & Finnegan, D. L. (1987). Volatilisation, transport and sublimation of metallic and non-metallic elements in high temperature gases at Merapi Volcano, Indonesia. *Geochimica et Cosmochimica Acta*, *51*, 2083–2101.
- Them, T. R., Gill, B. C., Cruthers, A. H., Gerhardt, A. M., Gröcke, D. R., Lyons, T. W., et al. (2018). Thallium isotopes reveal protracted anoxia during the Toarcian (Early Jurassic) associated with volcanism, carbon burial, and mass extinction. *Proceedings of the National Academy of Sciences*, *115*, 6596–6601.
- Them, T. R., Jagoe, C. J., Caruthers, A. H., Gill, B. C., Grasby, S. E., Gröcke, D. R., et al. (2019). Terrestrial sources as the primary delivery mechanism of mercury to the oceans across the Toarcian Oceanic Anoxic Event (Early Jurassic). *Earth and Planetary Science Letters*, *507*, 62–72.
- Tribouillard, N., Algeo, T. J., Lyons, T., & Ribolleau, A. (2006). Trace metals as paleoredox and paleoproductivity proxies: An update. *Chemical Geology*, *232*, 12–32.
- Turekian, K. K., & Wedepohl, K. H. (1961). Distribution of the elements in some major units of the Earth's crust. *The Geological Society of America Bulletin*, *72*, 175–192.
- Wang, X., Cawood, P. A., Zhao, H., Zhao, H., Grasby, S. E., Chen, Z.-Q., et al. (2018). Mercury anomalies across the end Permian mass extinction in South China from shallow and deep water depositional environments. *Earth and Planetary Science Letters*, *496*, 159–167.
- Wang, X., Cawood, P. A., Zhao, H., Zhao, L., Grasby, S. E., Chen, Z.-Q., & Zhang, L. (2019). Global mercury cycle during the end-Permian mass extinction and subsequent Early Triassic recovery. *Earth and Planetary Science Letters*, *513*, 144–155.
- Wignall, P. B. (2015). *The worst of times: How life on earth survived 80 million years of extinction*, Princeton and Oxford: : Princeton University Press.
- Wignall, P. B., Bond, D. P. G., Sun, Y., Grasby, S. E., Beauchamp, B., Joachimski, M., & Blomeier, D. P. G. (2016). Ultra-shallow marine anoxia in an Early Triassic shallow-marine clastic ramp (Spitsbergen) and the suppression of benthic radiation. *Geological Magazine*, *153*, 316–331.
- Wignall, P. B., & Hallam, A. (1992). Anoxia as a cause of the Permian/Triassic extinction: Facies evidence from northern Italy and the western United States. *Palaeogeography, Palaeoclimatology, Palaeoecology*, *93*, 21–46.
- Wignall, P. B., Morante, R., & Newton, R. (1998). The Permo-Triassic transition in Spitsbergen: $\delta^{13}\text{C}_{\text{org}}$ chemostratigraphy, Fe and S geochemistry, facies, fauna and trace fossils. *Geological Magazine*, *135*, 47–62.
- Wignall, P. B., & Twitchett, R. J. (1996). Oceanic anoxia and the end-Permian mass extinction. *Science*, *272*, 1155–1158.
- Zelenski, M. E., Fischer, T. P., de Moor, J. M., Marty, B., Zimmermann, L., Ayalew, D., et al. (2013). Trace elements in the gas emissions from the Erta Ale volcano, Afar, Ethiopia. *Chemical Geology*, *357*, 95–116.
- Zelenski, M. E., Malik, N., & Taran, Y. (2014). Emissions of trace elements during the 2012-2013 effusive eruption of Tolbachik Volcano, Kamchatka: Enrichment factors, partition coefficients and aerosol contribution. *Journal of Volcanology and Geothermal Research*, *285*, 136–149.